

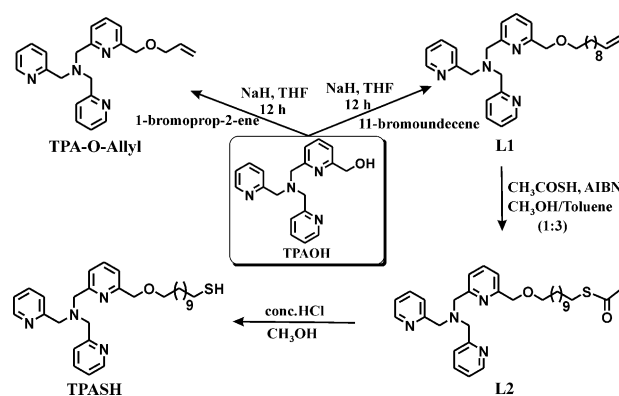
Surface Functionalization

Enhanced Reactivity of a Biomimetic Iron(II) α -Keto Acid Complex through Immobilization on Functionalized Gold Nanoparticles**

Debobrata Sheet, Partha Halder, and Tapan Kanti Paine*

Immobilization of transition-metal complexes by surface functionalization of gold nanoparticles (AuNPs) has recently attracted the attention for several applications.^[1] Thiol-protected AuNPs^[2] are stable and soluble in organic solvents. Therefore, immobilization of metal complexes on AuNPs permits reactions in common organic solvents and also induces properties of the metal complex to the NP.^[3] AuNPs functionalized by thiol-appended transition metal complexes are expected to find applications as immobilized catalysts to bridge between homogeneous and heterogeneous catalysis. The high surface area of a nanocatalyst increases the contact between the reactant and catalyst dramatically. These catalysts are easy to synthesize through desired surface modification and can be characterized by different analytical and spectroscopic techniques. Moreover, the catalyst can easily be separated from the reaction mixture. Several reports are now available where immobilization of metal catalysts on AuNPs has been shown to increase the catalytic reactivity.^[4] Improved catalytic activities of transition-metal catalysts through surface functionalization of AuNPs have inspired us to initiate a project on immobilization of biomimetic iron complexes. In this direction, we have investigated the dioxygen reactivity of nonheme iron complexes on functionalized AuNPs. Dioxygen-activating α -ketoglutarate (α -KG)-dependent oxygenases that carry out versatile biological reactions are well-studied in biology and biomimetic chemistry.^[5] The iron(II) centers of the enzymes activate dioxygen, upon binding of a bidentate α -KG and the substrate, to form an iron–oxygen intermediate.^[6] The heterolytic O–O bond cleavage of the intermediate results in formation of an iron(IV)–oxo oxidant to affect substrate oxidations. Iron(IV)–oxo intermediates have been trapped and characterized in studies with several α -ketoglutarate-dependent enzymes.^[7] In biomimetic chemistry, a number of iron(II)– α -keto acid complexes have been reported as functional models of α -ketoglutarate-dependent oxygenases.^[8] The model complexes exhibit versatile reactivity towards dioxygen and, in some cases, iron(IV)–oxo intermediates have been intercepted in the decarboxylation of α -keto acids. Model iron(II)– α -keto acid complexes of N_4 donor ligands have been

reported to react with O_2 for days to undergo stoichiometric decarboxylation of the coordinated α -keto acids.^[8a] Moreover, they often form μ -oxo diiron(III) complex at the end of the decarboxylation reaction, leading to the deactivation of the complex.^[8a] Such deactivation reaction may be avoided with a properly immobilized complex on the surface of AuNPs and is expected to exhibit improved/catalytic reactivity upon immobilization. As an outcome of our investigation, we report herein an enhanced reactivity of a biomimetic iron(II)–benzoylformate complex of a thiol-appended N_4 ligand (TPASH, Scheme 1) towards dioxygen upon immobi-



Scheme 1. Ligands used in this study. AIBN = azobis(isobutyronitrile).

lization on functionalized AuNPs. The reactivity of the immobilized complex is compared with that of a related iron(II)–benzoylformate complex supported by a tetradentate nitrogen-donor ligand, TPA-O-allyl (Scheme 1).

The tetradentate ligand TPA-O-allyl was synthesized from [6-(hydroxymethyl)-2-pyridylmethyl]bis(2-pyridylmethyl)amine (TPAOH)^[9] according to Scheme 1. The iron(II)– α -keto acid complex [(TPA-O-allyl)₂Fe₂(BF)₂](ClO₄)₂ (**1**) (where BF = monoanionic benzoylformate) was isolated from the reaction of TPA-O-allyl, Fe(ClO₄)₂·xH₂O, and NaBF in methanol (see the Experimental Section in the Supporting Information). The complex displays a paramagnetically shifted ¹H NMR spectrum in CDCl₃ indicating the high-spin nature of the iron(II) center (Supporting Information, Figure S1). The ESI-MS (in positive-ion mode, CH₃CN) of the complex shows an ion peak at *m/z* = 565.2 with the isotope distribution pattern calculated for the [(TPA-O-allyl)Fe(BF)]⁺ ion (Figure 1). The solid-state structure of the complex cation, however, displays a symmetrical dinuclear complex in which each iron(II) center is coordinated by a ligand and two carboxylate oxygen donors from two

[*] D. Sheet, Dr. P. Halder, Dr. T. K. Paine
Department of Inorganic Chemistry
Indian Association for the Cultivation of Science
2A & 2B Raja S. C. Mullick Road, Jadavpur, Kolkata-700032 (India)
E-mail: ictkp@iacs.res.in

[**] T.K.P. acknowledges the DST, Govt. of India (Project SR/S1/IC-51/2010) for financial support. D.S. thanks CSIR, India, for a fellowship.

Supporting information for this article is available on the WWW under <http://dx.doi.org/10.1002/anie.201305994>.

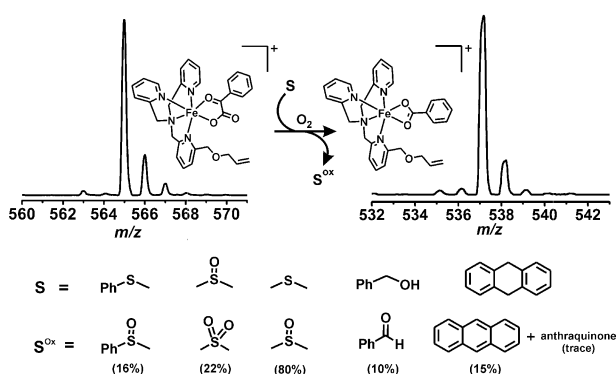


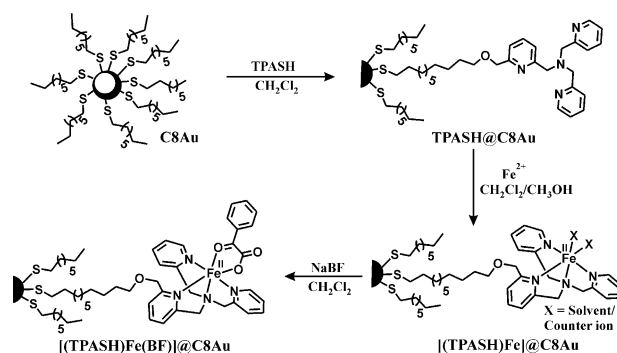
Figure 1. ESI-MS spectra (positive-ion mode, CH_3CN) of **1** (left) and the final oxidized species after the reaction of **1** with dioxygen at 295 K. The substrates (**S**) and their oxidized products (**S^{ox}**) are shown at the bottom. The values at the parenthesis indicate the oxidation product yields.

benzoylformates (Figure S2). The iron–nitrogen and iron–oxygen bond distances are typical of high-spin iron(II) complexes (Table S1). Two benzoylformates bridge between the two iron centers through the carboxylate groups. The optical spectrum of complex **1** in dichloromethane displays a broad MLCT band (Fe^{II} to π^* of the keto group) between 450 nm and 620 nm, suggesting a bidentate chelation of the α -keto acid (BF) to the iron(II) center by one keto oxygen and the carboxylate oxygen in solution. A lower extinction coefficient of the MLCT band may be attributed to the existence of an equilibrium between iron(II)–BF complexes with different binding modes (bidentate, monodentate, and bridging) of BF in solution.^[8a] Upon exposure of a dichloromethane solution of the complex to dioxygen the MLCT band gradually decreases (Figure S3) over a period of 24 h, indicating oxidation of the complex. The final reaction solution exhibits an ion peak at $m/z = 537.2$ attributable to the $[(\text{TPA-O-allyl})\text{Fe}(\text{benzoate})]^+$ ion (Figure 1). Time-dependent ^1H NMR data also support the oxidative decarboxylation of BF to benzoic acid slowly over 24 h (Figure S4). The GC-MS spectrum of methyl ester of benzoic acid exhibits ion peak at $m/z = 136$. When the reaction is carried out with $^{18}\text{O}_2$, the ion peak is shifted to $m/z = 138$, confirming incorporation of one oxygen atom from molecular oxygen into benzoic acid (Figure S5). An active iron–oxo oxidant is intercepted by external substrates such as thioanisole, dimethylsulfoxide, dimethyl sulfide, benzyl alcohol, and 9,10-dihydroanthracene (Figure 1; Supporting Information, Figures S6, S7).

For immobilization of the iron(II)–benzoylformate complex on AuNPs, an alkanethiol terminated in the tripodal N_4 ligand (TPASH) was synthesized (Scheme 1). Octanethiol-capped NP, C8Au (1–5 nm) were isolated according to the procedure reported by Brust et al.^[2a,b] by the reaction of gold(III) chloride and alkanethiol using a phase-transfer catalyst and subsequent reduction with sodium borohydride. Elemental analysis data of C8Au exhibits an Au/S molar ratio of 2.52:1, and the calculated C/H and C/S ratio indicate the capping of octanethiol on gold surface within experimental uncertainties. A composition of $(\text{Au})_{37}(\text{C8})_{14}$ for the cluster is

derived from the elemental analysis data. The XPS data for C8Au reveals the presence of gold, carbon, and sulfur, and the XPS signature of Au4f doublet with the peak-to-peak distance of 3.7 eV indicates the gold to be in Au^0 state (Figure S8).^[2a,10]

The TPASH-immobilized NPs, TPASH@C8Au, were isolated by place-exchange reaction after incubation of TPASH (2 equiv) and C8Au (1 equiv) for 36 h at 25 °C in dichloromethane (Scheme 2).^[11] Elemental analysis data of TPASH@C8Au indicate an Au/S molar ratio of 2.78:1. The experimental C/N and C/H ratio clearly illustrate the immobilization of TPASH. The surface coverage of the NP with TPASH was estimated by an ^1H NMR integration using 1,4-benzoquinone as an internal standard (Figure S9). An estimated 0.002 mmol of TPASH were immobilized on 10 mg of TPASH@C8Au with an effective molar ratio of TPASH:C8Au being 1:9. On the basis of these results, a composition of $(\text{Au})_{37}(\text{C8})_9(\text{TPASH})$ has been formulated for TPASH@C8Au.



Scheme 2. Functionalization of gold nanoparticles with N_4 ligand and iron complexes.

The functionalization of AuNPs by iron(II) complex was made by the reaction of TPASH@C8Au with iron(II) perchlorate in dichloromethane (Scheme 2). After immobilization of iron, the NPs became soluble in acetonitrile, indicating the formation of charged species. The metal ion was easily incorporated owing to strong chelating ability of the pyridine nitrogen atoms of the ligand with the iron center. The reaction of immobilized iron(II) complex with NaBF in dichloromethane–methanol afforded $[(\text{TPASH})\text{Fe}(\text{BF})]@\text{C8Au}$ (**2**) (Scheme 2).

The functionalization of AuNPs by iron complex is supported by the IR spectrum of $[(\text{TPASH})\text{Fe}]@\text{C8Au}$, which exhibits a peak owing to perchlorate counterions at 1116 cm^{-1} . Additionally, in **2**, two peaks at 1602 and 1640 cm^{-1} indicate the binding of BF with the iron(II) center (Figure S10). In the optical spectra, all the NP exhibit broad surface plasmon band at around 520 nm (Figure 2).^[2d,12] After complexation with iron(II), a slight shift in the surface plasmon band of TPASH@C8Au is observed with the appearance of a shoulder between 365–382 nm. Upon binding of BF to the iron center a new shoulder appears at 304 nm along with broad shoulder at 375 nm (Figure 2, inset). The band at 368 nm could be attributed to the MLCT band from

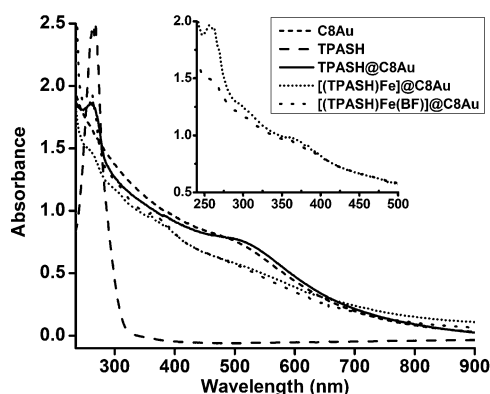


Figure 2. Absorption spectra of functionalized gold nanoparticles in dichloromethane at 295 K.

Fe^{II} to pyridine typically observed in Fe^{II} -TPA complexes. The binding mode of BF to the iron center in **2** could not be analyzed by optical spectroscopy owing to a high molar extinction coefficient of the SP band as compared to the Fe^{II} -to-keto charge transfer band. The ^1H NMR spectrum of C8Au exhibits broad peaks at 0.88 and 1.27 ppm. The peaks corresponding to TPASH are broadened upon immobilization on C8Au (Figure S9). A paramagnetically shifted ^1H NMR spectrum is observed for $[(\text{TPASH})\text{Fe}]\text{@C8Au}$, with a large downfield shift of the Py (β, β') protons (Figure S11). The appearance of paramagnetically shifted broad peaks at 10–17 ppm for **2** suggests the binding of BF to the iron center of $[(\text{TPASH})\text{Fe}]\text{@C8Au}$. Thermogravimetric data also support the incorporation of iron-BF complex on the surface of NP with the Au-S bonds being stable up to 200 °C (Figure S12). The XPS signature of **2**, consisting of a Au 4f doublet with a peak-to-peak distance of 3.7 eV, indicates that gold is in the Au^0 state (Figure S13).

PXRD data of the NP exhibit patterns similar to that of fcc Au (Figure S14). The broad patterns and the disappearance of (200) plane reveal that all the NPs are less than 5 nm in diameter.^[10,13] HRTEM images reveal the polycrystalline nature of the AuNP (Figure S15 and S16). The attachment of thiol unit to the gold was further characterized by EDAX, which supports the presence of C, N, S, and Au in the functionalized NPs. The histogram indicates that the maximum number of particles are in the range of 2–5 nm for C8Au (Figure S16a).^[2d] The particle core size remains almost unaltered and well dispersed without any sign of agglomeration upon immobilization of TPASH (Figure S15a). The HRTEM images reveal that the interparticle distances increase upon introduction of iron(II) ions (Figure S15b). The NPs are stabilized upon coordination with the metal ion, and the resulting charge prevents agglomeration.^[14] Interestingly, binding of BF to the immobilized iron complex does not affect the particle size; rather the NPs are further stabilized, as depicted from TEM images (Figure S16b).

$[(\text{TPASH})\text{Fe}(\text{BF})]\text{@C8Au}$ (**2**) reacts with dioxygen to undergo oxidative decarboxylation of the coordinated benzoylformate (BF) to afford benzoic acid as the only product. Time-dependent ^1H NMR spectra reveal a quantitative formation of benzoic acid in 2 h (Figure 3). Interestingly, the rate

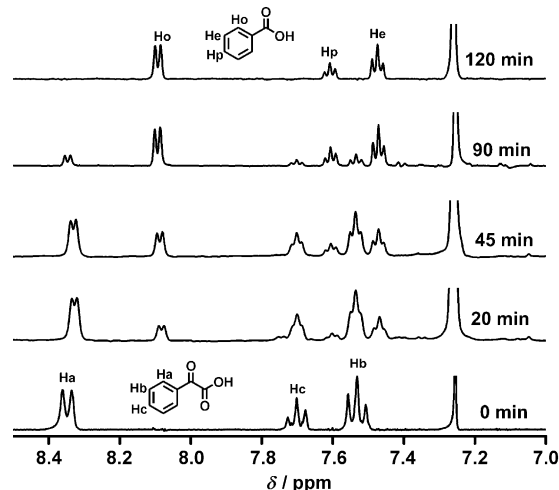
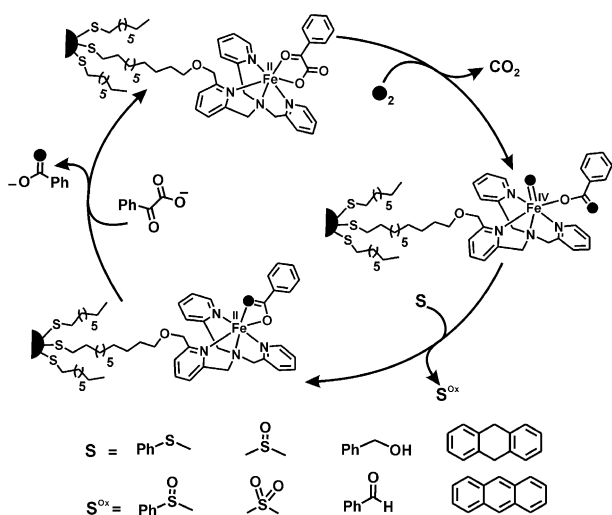


Figure 3. Time-dependent ^1H NMR spectra (500 MHz, CDCl_3 , 295 K) during the reaction of **2** with O_2 .

of decarboxylation of BF to benzoic acid for the immobilized complex (**2**) is found to be 8 times faster than **1**, about 20 times faster than $[(\text{TPA})\text{Fe}^{\text{II}}(\text{BF})]^+$, and 50 times faster than $[(6\text{Me}_3\text{TPA})\text{Fe}^{\text{II}}(\text{BF})]^+$.^[8a] It has been reported that NPs protected by thiols are unreactive towards oxygen.^[15] A number of control experiments were performed to establish the inertness of NP towards dioxygen. No decarboxylation of BF could be observed when 1) C8Au (25 mg) was reacted with NaBF (0.005 mmol) in dichloromethane and acetone for 16 h; 2) C8Au (25 mg) was treated with NET_3 (0.005 mmol) and HBF (0.005 mmol) in dichloromethane and acetone for 16 h; and 3) C8Au (25 mg), NaBF (0.005 mmol), and $\text{Fe}(\text{ClO}_4)_2 \cdot x\text{H}_2\text{O}$ (0.005 mmol) were reacted together for 16 h. On the basis of the above results, it may safely be concluded that the dramatic increase in the rate of BF decarboxylation is a result of immobilization of the complex on AuNPs, which provides large surface area and the self-assembly providing spherical curvature with open access of the active iron center for faster reactivity.

To intercept the active iron-oxygen species formed upon decarboxylation of **2**, some external reagents were used as indirect probes. Thioanisole, dimethyl sulfoxide, benzyl alcohol, and 9,10-dihydroanthracene could intercept the active iron-oxo oxidant, affording thioanisole oxide (20%), dimethyl sulfone (60%), benzaldehyde (30%), and anthracene (30% and a small amount of anthraquinone), respectively, in the reaction of **2** with dioxygen in acetone (Scheme 3; Supporting Information, Figure S17). With all of these substrates, the yield of benzoic acid is found to be quantitative. The GC-MS spectrum exhibits ion peak of thioanisole oxide at $m/z = 140$, which is shifted two mass unit higher in the presence of $^{18}\text{O}_2$ (Figure S18). A labeling experiment further confirmed incorporation of another oxygen atom into benzoic acid (Figure S19).

The high valent oxo species, formed on the AuNP surface, is thus capable of transferring oxo atom to substrate to carry out oxidation reactions (Scheme 3). An IR spectrum of the NP isolated after oxidation exhibits a similar spectral feature



Scheme 3. Oxidative decarboxylation of benzoylformic acid by an iron complex on functionalized gold nanoparticles.

as in **2** (Figure S20). The SP band at 520 nm for **2** remains almost similar, suggesting that oxidation does not really affect the AuNP surface (Figure S21). GC-MS analysis immediately after oxidation suggests about 5% leaching of the adsorbed thiolates. The TEM image suggests the recycled NPs to be within 5 nm without any agglomeration (Figure S22). The XRD pattern (Figure S23) after oxidation is similar to the XRD pattern of **2**. All of these results strongly support the robustness of the biomimetic complex on functionalized AuNPs and the immobilized complex can return into the cycle for catalytic conversion.

Preliminary studies on the catalytic reactivity were carried out with **2** (10 mg, 0.002 mmol) in the presence of excess NaBF and thioanisole in $\text{CH}_2\text{Cl}_2/\text{CH}_3\text{CN}$ mixture or in acetone at room temperature (Table 1). Complex **2** was found to catalyze the oxo-atom transfer to thioanisole in the presence of excess BF, which put back the dioxygen activating species into the catalytic cycle (Scheme 3). It is important to mention here that complex **1** does not exhibit any catalytic reactivity under similar experimental conditions (Table 1).

Table 1: Catalytic reactivity of **2**.

Complex (amount)	Solvent	NaBF [equiv]	t [h]	TON ^[d]
2 ^[a] (10 mg)	acetone	3	8	2
2 ^[a] (10 mg)	acetone	5	8	4
2 ^[a] (10 mg)	acetone	10	8	5
2 ^[a] (10 mg)	acetone	20	8	6
2 ^[a] (10 mg)	$\text{CH}_2\text{Cl}_2/\text{CH}_3\text{CN}$	5	8	3
2 ^[a] (10 mg)	$\text{CH}_2\text{Cl}_2/\text{CH}_3\text{CN}$	10	8	5
1 ^[b] (1.3 mg)	CH_3CN	5	8	0
1 ^[b] (1.3 mg)	CH_3CN	10	24	0
1 ^[b] (1.3 mg)	CH_3CN	5	48	0
1 ^[c] (13 mg)	CH_3CN	5	48	0

[a] Reaction conditions: 10 mg (0.002 mmol) catalyst, 100 equiv (0.2 mmol) of substrate (thioanisole). [b] Conditions: 1.3 mg (0.002 mmol) complex, 100 equiv (0.2 mmol) of substrate (thioanisole). [c] Conditions: 13 mg (0.02 mmol) complex, 100 equiv (2 mmol) of substrate (thioanisole). [d] The TON was calculated on the basis of the percentage of benzoic acid formed from excess NaBF used.

The reactivity remains stoichiometric even in the presence of higher concentration of complex **1**. The immobilized complex therefore proved to be a catalyst showing a highest TON of 6 using dioxygen as the terminal oxidant. The TON obtained with the immobilized complex is an outcome of the barrier caused by the functionalized AuNPs for the formation of any inactive dimeric iron complex. GC-MS analysis after 12 h under catalytic conditions suggests the formation of dioctyl disulfide in about 15% yield indicating the leaching of adsorbed thiolates. Leaching of the gold surface is also evident from the TEM image after catalysis (Figure S24).

In conclusion, we have reported the synthesis and characterization of a surface-immobilized nonheme iron complex. The reactivity of the NP functionalized with terminated N_4 ligand is enhanced considerably compared to its non-immobilized analogue. Moreover, the immobilized complex exhibits catalytic reactivity in the presence of excess substrates. The increased reactivity can be accounted for the surface properties providing suitable orientation and larger surface area that favor enhanced interaction. The confinement of the complex may also exert cooperativity. The proof-of-concept system reported herein show potential and would provide useful insight in developing a bioinspired immobilized catalyst. Place-exchange with a long-chain alkanethiol with metal complexes terminated at a shorter chain is expected to create a protective environment at the catalytic metal center to provide selectivity for biomimetic oxidative transformations. Further tuning of the immobilized complex to increase the catalytic efficiency is presently being pursued in our laboratory.

Received: July 10, 2013

Revised: September 29, 2013

Published online: October 18, 2013

Keywords: α -keto acids · catalysis · dioxygen · gold nanoparticles · iron

- [1] a) J. D. E. T. Wilton-Ely, *Dalton Trans.* **2008**, 25; b) S. Roy, M. A. Pericàs, *Org. Biomol. Chem.* **2009**, 7, 2669; c) E. K. Beloglazkina, A. G. Majouga, R. B. Romashkina, N. V. Zyk, N. S. Zefirov, *Russ. Chem. Rev.* **2012**, 81, 65.
- [2] a) M. Brust, M. Walker, D. Bethell, D. J. Schiffrin, R. Whyman, *J. Chem. Soc. Chem. Commun.* **1994**, 801; b) M. Brust, J. Fink, D. Bethell, D. J. Schiffrin, C. Kiely, *J. Chem. Soc. Chem. Commun.* **1995**, 1655; c) A. C. Templeton, W. P. Wuelfing, R. W. Murray, *Acc. Chem. Res.* **2000**, 33, 27; d) M.-C. Daniel, D. Astruc, *Chem. Rev.* **2004**, 104, 293.
- [3] a) P. D. Beer, D. P. Cormode, J. J. Davis, *Chem. Commun.* **2004**, 414; b) D. Samanta, N. Faure, F. Rondelez, A. Sarkar, *Chem. Commun.* **2003**, 1186; c) M. Alvaro, C. Aprile, B. Ferrer, F. Sastre, H. García, *Dalton Trans.* **2009**, 7437; d) C. R. Mayer, G. Cucchiaro, J. Jullien, F. Dumur, J. Marrot, E. Dumas, F. Sécheresse, *Eur. J. Inorg. Chem.* **2008**, 3614; e) S. Wang, W.-S. Sim, *Langmuir* **2006**, 22, 7861; f) T. B. Norsten, B. L. Frankamp, V. M. Rotello, *Nano Lett.* **2002**, 2, 1345; g) P. Pramod, P. K. Sudeep, K. G. Thomas, P. V. Kamat, *J. Phys. Chem. B* **2006**, 110, 20737.
- [4] a) M. Bartz, J. Küther, R. Seshadri, W. Tremel, *Angew. Chem.* **1998**, 110, 2646; *Angew. Chem. Int. Ed.* **1998**, 37, 2466; b) H. Li, Y.-Y. Luk, M. Mrksich, *Langmuir* **1999**, 15, 4957; c) K. Mar-

- ubayashi, S. Takizawa, T. Kawakusu, T. Arai, H. Sasai, *Org. Lett.* **2003**, *5*, 4409; d) T. Belser, M. Stöhr, A. Pfaltz, *J. Am. Chem. Soc.* **2005**, *127*, 8720; e) R. Bonomi, F. Selvestrel, V. Lombardo, C. Sissi, S. Polizzi, F. Mancin, U. Tonellato, P. Scrimin, *J. Am. Chem. Soc.* **2008**, *130*, 15744.
- [5] a) M. Costas, M. P. Mehn, M. P. Jensen, L. Que, Jr., *Chem. Rev.* **2004**, *104*, 939; b) R. P. Hausinger, *Crit. Rev. Biochem. Mol. Biol.* **2004**, *39*, 21.
- [6] J. M. Elkins, M. J. Ryle, I. J. Clifton, J. C. D. Hotopp, J. S. Lloyd, N. I. Burzlaff, J. E. Baldwin, R. P. Hausinger, P. L. Roach, *Biochemistry* **2002**, *41*, 5185.
- [7] a) A. R. McDonald, L. Que, Jr., *Coord. Chem. Rev.* **2013**, *257*, 414; b) C. Krebs, D. G. Fujimori, C. T. Walsh, J. M. Bollinger, Jr., *Acc. Chem. Res.* **2007**, *40*, 484; c) D. P. Galonić, E. W. Barr, C. T. Walsh, J. M. Bollinger, Jr., C. Krebs, *Nat. Chem. Biol.* **2007**, *3*, 113; d) S. Sinnecker, N. Svensen, E. W. Barr, S. Ye, J. M. Bollinger, Jr., F. Neese, C. Krebs, *J. Am. Chem. Soc.* **2007**, *129*, 6168; e) M. L. Matthews, C. M. Krest, E. W. Barr, F. H. Vaillancourt, C. T. Walsh, M. T. Green, C. Krebs, J. M. Bollinger, Jr., *Biochemistry* **2009**, *48*, 4331; f) D. Galonić Fujimori, E. W. Barr, M. L. Matthews, G. M. Koch, J. R. Yonce, C. T. Walsh, J. M. Bollinger, Jr., C. Krebs, P. J. Riggs-Gelasco, *J. Am. Chem. Soc.* **2007**, *129*, 13408.
- [8] a) Y.-M. Chiou, L. Que, Jr., *J. Am. Chem. Soc.* **1995**, *117*, 3999; b) E. H. Ha, R. Y. N. Ho, J. F. Kisiel, J. S. Valentine, *Inorg. Chem.* **1995**, *34*, 2265; c) M. P. Mehn, K. Fujisawa, E. L. Hegg, L. Que, Jr., *J. Am. Chem. Soc.* **2003**, *125*, 7828; d) A. Mukherjee, M. A. Cranswick, M. Chakrabarti, T. K. Paine, K. Fujisawa, E. Münck, L. Que, Jr., *Inorg. Chem.* **2010**, *49*, 3618; e) T. K. Paine, H. Zheng, L. Que, Jr., *Inorg. Chem.* **2005**, *44*, 474; f) O. Das, S. Chatterjee, T. K. Paine, *J. Biol. Inorg. Chem.* **2013**, *18*, 401.
- [9] Z. He, P. J. Chaimungkalanont, D. C. Craig, S. B. Colbran, *J. Chem. Soc. Dalton Trans.* **2000**, 1419.
- [10] D. V. Leff, L. Brandt, J. R. Heath, *Langmuir* **1996**, *12*, 4723.
- [11] a) M. J. Hostetler, S. J. Green, J. J. Stokes, R. W. Murray, *J. Am. Chem. Soc.* **1996**, *118*, 4212; b) M. J. Hostetler, A. C. Templeton, R. W. Murray, *Langmuir* **1999**, *15*, 3782; c) R. S. Ingram, M. J. Hostetler, R. W. Murray, *J. Am. Chem. Soc.* **1997**, *119*, 9175.
- [12] a) P. Mulvaney, *Langmuir* **1996**, *12*, 788; b) A. C. Templeton, J. J. Pietron, R. W. Murray, P. Mulvaney, *J. Phys. Chem. B* **2000**, *104*, 564.
- [13] D. V. Leff, P. C. Ohara, J. R. Heath, W. M. Gelbart, *J. Phys. Chem.* **1995**, *99*, 7036.
- [14] a) M. Montalti, L. Prodi, N. Zaccheroni, M. Beltrame, T. Morotti, S. Quici, *New J. Chem.* **2007**, *31*, 102; b) F. S. Nunes, L. D. S. Bonifácio, K. Araki, H. E. Toma, *Inorg. Chem.* **2006**, *45*, 94.
- [15] P. Ionita, M. Conte, B. C. Gilbert, V. Chechik, *Org. Biomol. Chem.* **2007**, *5*, 3504.